# Thermal stability of metal Ohmic contacts in indium gallium zinc oxide transistors using a graphene barrier layer

Jeong Eun Lee,[1,a)] Bhupendra K. Sharma,[2,a)] Seoung-Ki Lee,[1] Haseok Jeon,[1] Byung Hee Hong,[3] Hoo-Jeong Lee,[1,b)] and Jong-Hyun Ahn[2,b)]

[1]School of Advanced Materials Science and Engineering, Sungkyunkwan University, Suwon 440-746, Korea
[2]School of Electrical & Electronic Engineering, Yonsei University, Seoul 120-749, Korea
[3]Department of Chemistry, Seoul National University, Seoul 151-747, Korea

The excellent impermeability of graphene was exploited to produce stable ohmic contact at the interface between Al metal and a semiconducting indium gallium zinc oxide (IGZO) layer after high-temperature annealing. Thin film transistors (TFTs) were fabricated with and without a graphene interlayer between the Al metal and the IGZO channel region. Metal contact at the interface prepared without a graphene interlayer showed serious instabilities in the IGZO TFT under thermal annealing; however, the insertion of a graphene interlayer between the IGZO channel and the Al metal offered good stability under repeated high-temperature annealing cycles and maintained ohmic contact. © 2013 American Institute of Physics. [http://dx.doi.org/10.1063/1.4796174]

Recently, graphene, which comprises a two-dimensional (2D) network of sp$^2$ hybridized carbon atoms packed into hexagonal structure, has attracted a great deal of attention due to a long-range ordered $\pi$-conjugation structure that provides excellent thermal,[1] electrical,[2] and mechanical[3] properties. Significant efforts have been applied toward the use of graphene as an electrode or channel region toward the fabrication of flexible electronic devices. Graphene is chemically stable and exhibits excellent gas impermeability, even toward the smallest gas molecules, such as He, owing to the densely packed hexagonal lattice of electron clouds.[4–9] This suggests that graphene films are potentially useful as a gas barrier for the prevention of absorption/desorption, inter-diffusion between two metals at an interface, or oxidation at a metal surface. The oxidation of metal contacts at the interface of a source–drain region has been a longstanding obstacle to the preparation of oxide-based thin film transistors (TFTs). Oxidation significantly degrades device performance. For exploiting the great impermeable property of graphene, it is quite important to check its potentiality in TFT devices.

Indium gallium zinc oxide (IGZO) semiconductors have attracted attention over the last decade for their applications in the driver elements of a variety of emerging display technologies, such as active matrix organic light emitting diodes (AMOLEDs) or three-dimensional liquid crystal displays.[10–16] Although IGZO TFTs have a lower mobility than polycrystalline Si-based TFTs formed by excimer laser annealing, the mobility (over 10 cm$^2$/Vs)[17–19] exceeds that of a-Si TFTs and is more than sufficient to drive an OLED. In addition, IGZO is amenable to low-temperature deposition,[20–23] which enables the use of low-cost soda lime substrates or even flexible plastics,[24–31] and it may be fabricated over large substrates using conventional a-Si TFT manufacturing lines. Currently, IGZO TFTs are limited in their utility in OLED display backplanes. This application requires the development of highly conductive metal electrodes that can form good contact interfaces with IGZO channels. Highly conductive metal electrodes enable the production of large, high-quality, low-cost AMOLED displays; however, oxygen diffusion from the IGZO films causes oxidation of the metal layers.[32,33] The oxide semiconductor TFTs then degrade as a result.

Figure 1(a) shows a schematic representation of the key steps involved in the fabrication process. An IGZO TFT array was fabricated on a heavily doped p-type Si substrate coated with a 100 nm SiO$_2$ layer. The 60 nm thick rectangles of IGZO were deposited using a 4-in. polycrystalline InGaZnO (1:1:1) target of 99.999 purity by RF-sputtering onto a cleaned SiO$_2$/Si substrate at room temperature. The substrate was then annealed in air at 350 °C for 1 h to improve the stability and crystalline order. A passivation SiO$_2$ layer (50 nm thick) was deposited onto the channel region alone using an E-beam evaporator. Graphene thin films were grown via chemical vapor deposition onto a Cu foil, after which the films were transferred using poly(methyl methacrylate) (PMMA) as the supporting layer. Three-layer graphene films were transferred to the source–drain region of the IGZO prior to the deposition of the Al metal to prevent oxidation of the Al due to oxygen gas diffusion from the IGZO. After depositing the Al metal onto the source–drain region, graphene layers above the channel region were etched away using reactive ion etching (at an O$_2$ concentration of 20 sccm). The quality of the graphene layers was investigated by Raman spectroscopy (Figure 1(b)) and current–voltage measurements (Figure 1(c)). The observation of "G" and "2D" peaks at 1580 and 2670 cm$^{-1}$ clearly indicated the successful synthesis of graphene films. The intensities of the peaks corresponding to the three-layer graphene films increased while the peak positions and intensity ratio of the "G" and "2D" peaks remained unchanged, indicating that the properties of the graphene film remained unchanged, even after stacking. The current–voltage characteristics show that

a)J. E. Lee and B. K. Sharma contributed equally to this work.
b)Authors to whom correspondence should be addressed. Electronic addresses: hlee@skku.edu and ahnj@yonsei.ac.kr

**(a)**



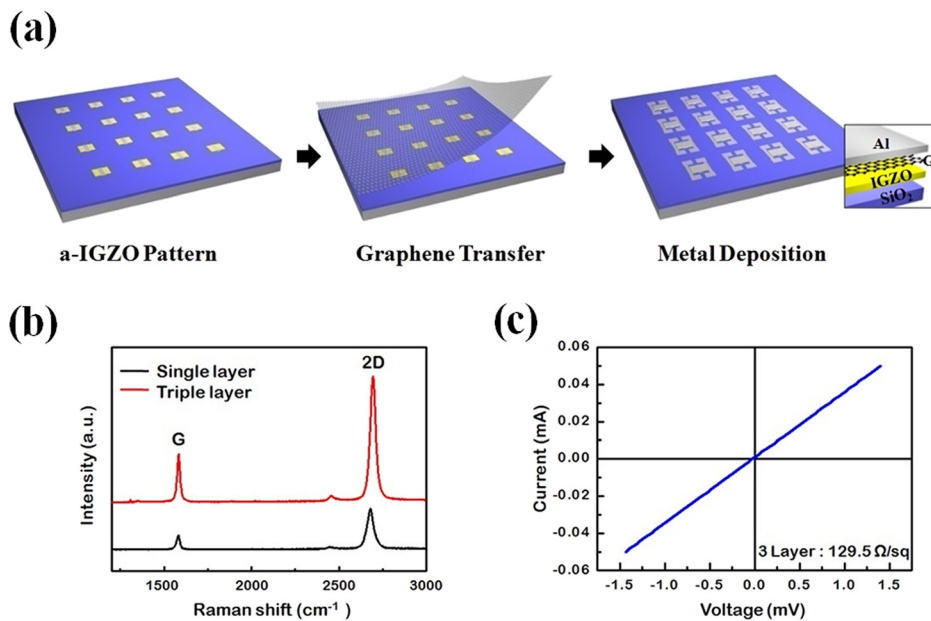a-IGZO Pattern        Graphene Transfer        Metal Deposition

**(b)**



**(c)**



FIG. 1. (a) Schematic illustration of the key steps involved in the fabrication of staggered bottom gated IGZO-based TFTs. A graphene film was inserted between the source–drain Al electrode and the IGZO channel. (b) Raman spectra of the transferred single- and triple-layer graphene on a SiO$_2$ wafer. (c) Current–voltage characteristic of the graphene films, showing the sheet resistance.

the synthesized graphene films were highly conductive, and the sheet resistance was 129 Ω/sq (Figure 1(c)).

The transfer characteristics of the IGZO TFTs prepared without and with a graphene interlayer between the IGZO channel and the Al metal contacts (S-D) for three different annealing cycles (1, 2, and 3) are shown in Figures 2(a) and 2(b), respectively, on a linear scale, and the corresponding semi-logarithmic plots without and with the graphene interlayer are shown in Figures 2(c) and 2(d), respectively. Initially, the IGZO TFT prepared without a graphene interlayer (A-IGZO) showed good transfer curves without annealing (cycle 0), exhibiting an on/off ratio (I$_{on/off}$) of $2.7 \times 10^7$ and a sub-threshold swing (SS) of 0.9 V/decade; however, these properties degraded more and more over repeated cycles of heat treatment at 250 °C. Contrasting with the behavior of the A-IGZO TFTs, the IGZO TFT with a graphene interlayer (AG-IGZO) initially displayed relatively poor transfer characteristics that improved under subsequent repeated heat treatment cycles. The poor performance of the AG-IGZO TFT sample prepared without annealing arose from the bad contact between the channel region (IGZO) and the transferred graphene layers, which improved as heat treatment was delivered. The annealing cycle conditions are shown in the inset of Figure 2(a). Initially, the temperature increased rapidly from room temperature to 250 °C, then was maintained for 5 min. The temperature then decreased rapidly to room temperature. This cycle was repeated three times. The rapid temperature increases and decreases were carried out to test the device's capabilities and durability. This type of heating cycle is more likely to be encountered than slow heating and cooling. After the first annealing cycle, I$_{on/off}$ decreased to $4.4 \times 10^6$ and SS increased to 1.1 V/decade for the A-IGZO TFT. These values then further degraded to $2.3 \times 10^6$ and 1.0 V/decade, and $1 \times 10^6$ and 2.0 V/decade for cycles 2 and 3, respectively. In the AG-IGZO TFTs, the I$_{on/off}$ ratio and SS values were found to be $8.0 \times 10^6$ and 2.0 V/decade without heat treatment, and these values improved after repeated heat treatment cycles. An optical image of a top-view of the device is shown in the
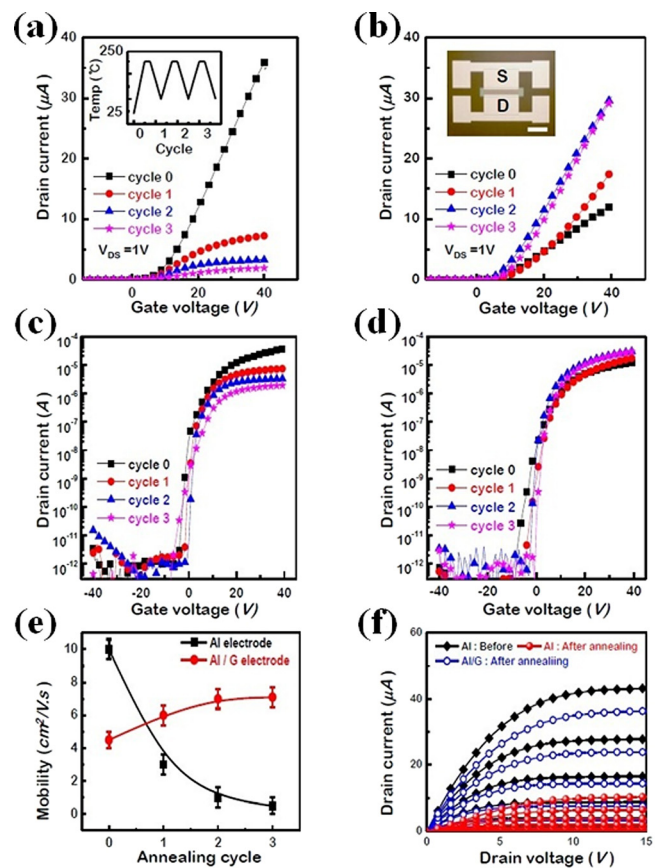


FIG. 2. Transfer characteristics before and after repeated high-temperature annealing cycles, shown on a linear scale ((a) and (b)) and on a semi-logarithmic scale ((c) and (d)), for the IGZO TFTs. (a) and (c) prepared without a graphene interlayer (A-IGZO) and (b) and (d) prepared with a graphene interlayer (AG-IGZO) between the S-D electrode and the IGZO channel. The inset of (a) shows the conditions used during the repeated annealing cycles and (b) shows a top-view optical image of a TFT (the scale bar denotes 100 $\mu$m). (e) The mobilities of the A-IGZO and AG-IGZO devices as a function of the annealing cycles. (f) Output characteristics of the A-IGZO device before and after annealing, and of the AG-IGZO device after annealing.

TABLE I. Electrical parameters characterizing the IGZO TFT prepared (i) without and (ii) with a graphene interlayer, after annealing. After the annealing cycles, the mobility of the IGZO TFT prepared without using a graphene interlayer degraded, whereas the mobility improved for the TFT prepared with a graphene interlayer inserted between the channel and the Al electrode.

| Nature of treatment | Field-effect mobility ($cm^2$/Vs) | Threshold voltage (V) | Subthreshold gate swing (V/decade) | On/off ratio |
|---|---|---|---|---|
| (i) | | | | |
| 0 cycle | 10.5 | 4.4 | 0.9 | $2.7 \times 10^7$ |
| 1 cycle | 3.0 | 3.6 | 1.1 | $4.4 \times 10^6$ |
| 2 cycle | 1.0 | 3.8 | 1.0 | $2.3 \times 10^6$ |
| 3 cycle | 0.5 | 4.3 | 2.0 | $1.0 \times 10^6$ |
| (ii) | | | | |
| 0 cycle | 4.5 | 4.7 | 2.0 | $8.0 \times 10^6$ |
| 1 cycle | 6.0 | 5.0 | 1.9 | $9.1 \times 10^6$ |
| 2 cycle | 7.0 | 4.0 | 0.8 | $1.7 \times 10^7$ |
| 3 cycle | 7.2 | 4.2 | 0.9 | $2.5 \times 10^7$ |

inset of Figure 2(b). The mobilities of the A-IGZO and AG-IGZO TFTs as a function of the annealing cycle are plotted in Figure 2(e). The initial mobilities of the A-IGZO and AG-IGZO TFTs without heat treatment were calculated to be 10.5 $cm^2$/Vs and 4.5 $cm^2$/Vs, respectively. After the heat treatment during cycle 1, the mobility of the A-IGZO TFTs decreased to 3.0 $cm^2$/Vs, whereas it increased to 6.0 $cm^2$/Vs for the AG-IGZO TFT. The mobility further decreased to 1.0 and 0.5 $cm^2$/Vs for the A-IGZO TFTs during annealing cycles 2 and 3. On the other hand, the mobility in the AG-IGZO TFTs first increased to 7.0 $cm^2$/Vs during annealing cycle 2, then remained relatively stable during further repeated annealing cycles. The performance degradation in TFTs prepared without a graphene interlayer after heat treatment was attributed to the oxidation of the metal contacts ($Al_2O_3$) at the interface region between the IGZO channel and the Al metal contacts, whereas the graphene interlayer in the AG-IGZO TFTs restricted oxidation of the Al metal at the interface region, thereby preserving the electrical performance, as revealed experimentally. The output characteristics of the A-IGZO TFTs before and after the heat treatment, and of the AG-IGZO TFTs after heat treatment, over a gate voltage range of 0–20 V with a step size of 2 V, are shown in Figure 2(f). The saturated output current levels of the A-IGZO TFTs clearly decreased by a factor of 4 after three annealing cycles, as compared to the output current levels obtained without heat treatment. The output-saturated current levels of the AG-IGZO TFT increased after heat treatment and were much larger than the A-IGZO TFT output current levels obtained after heat treatment, indicating that the graphene interlayer between the channel region IGZO and the Al metal contact acted as a perfect barrier for preventing Al metal oxidation, thereby maintaining the quality of the metal contact. Schottky contact at low voltages was observed in the output characteristic of the A-IGZO TFTs after the high-temperature annealing step of cycle 3 (not shown here). Therefore, oxidation yielded a higher contact resistance and hindered carrier transport in the A-IGZO TFTs submitted to heat treatment. The electrical parameters characterizing the A-IGZO and AG-IGZO TFTs before and after heat treatment are summarized in Table I.

The presence of Al oxidation in the A-IGZO TFT after annealing was confirmed by investigating the device microstructure using transmission electron microscopy (TEM). Figure 3 shows cross-sectional high-resolution TEM (HR-TEM) images of the Al/IGZO interface region before and after annealing of the IGZO TFTs prepared without (a, b) and with (c, d) a graphene interlayer. The cross-sectional images of the TFTs prepared without a graphene interlayer clearly revealed the formation of an oxidized layer at the Al/IGZO interface after heat treatment (Figure 3(b)). The thickness of the oxidative layer was approximately 7–8 nm, which was sufficient to hinder the transport of carriers through the Al/IGZO metal interface. Oxidation of the Al metal at the IGZO surface resulted from the diffusion of oxygen atoms from the semiconducting IGZO channel region to the Al metal after high-temperature annealing. The graphene interlayer at the
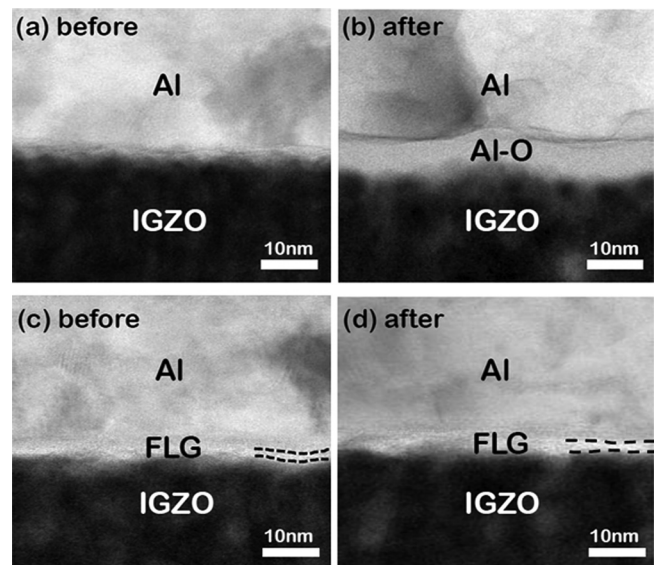


FIG. 3. Cross-sectional HRTEM images of an A-IGZO TFT (a) before and (b) after annealing cycle 3, which involved heating at 250 °C. The formation of an oxidative layer ($Al_2O_3$) at the Al/IGZO interface was apparent after annealing. The cross-sectional HRTEM images of AG-IGZO TFT (c) before and (d) after annealing cycle 3, revealed that the graphene films (FLG: few layer graphene) acted as perfect barriers to prevent O atom diffusion at the interface during annealing.
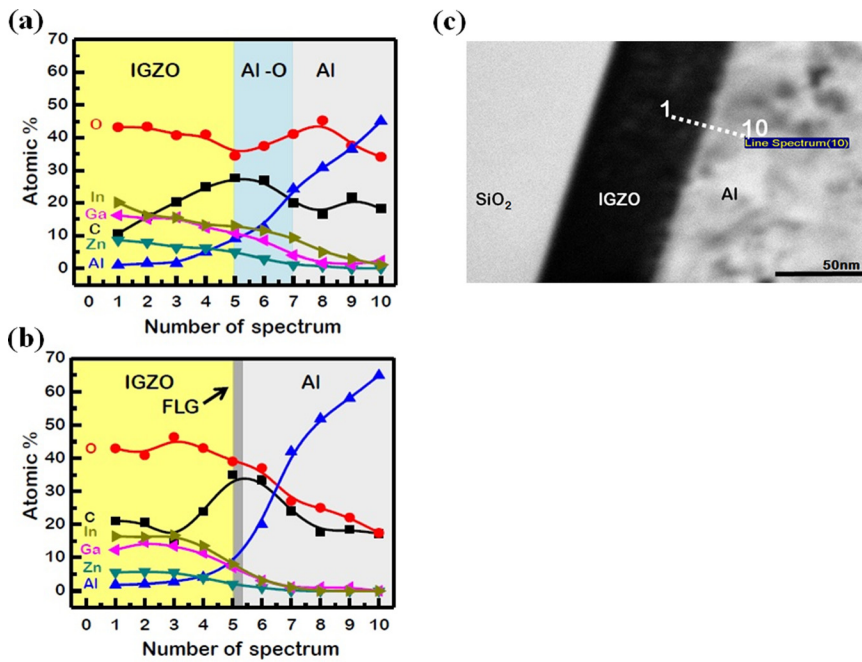
FIG. 4. (a) Energy dispersive X-ray photoelectron spectroscopic analysis, showing the atomic % of IGZO TFT prepared (a) without and (b) with a graphene interlayer between the S-D electrodes and channel after annealing at 250 °C. (c) TEM image of the SiO$_2$/IGZO/Al interfaces during scanning from deep within the IGZO channel to deep within the Al electrode covering the interfacial oxidative layer. EDS spectra were collected at 10 points over the scanning range (50 nm).

Al/IGZO metal interface before and after annealing could be seen clearly in the cross-sectional images of the TFTs (Figures 3(c) and 3(d)). The graphene layers between the IGZO channel and the Al metal contact acted as a perfect barrier to prevent the diffusion of oxygen atoms from the IGZO to the Al metal at the Al/IGZO interface.

Oxygen diffusion and its effect on the atomic concentration of various elements at Al/IGZO interface after annealing was further quantified by energy dispersive x-ray spectroscopic (EDS) analysis. The EDS spectrum was collected from the IGZO channel to the Al metal region, passing through the interface region. Figures 4(a) and 4(b) show the quantified EDS spectra of TFTs prepared without and with a graphene interlayer, after the annealing cycle 3. The atomic concentrations of the constituent elements (In, Ga, Zn, Al, and O) and C were monitored as a function of the sample depth, from the IGZO channel region to the Al metal contact. Initially, the EDS spectra of the TFTs without a graphene interlayer (Figure 4(a)) were dominated by In, Ga, Zn, and O, whereas the Al atomic concentration was negligible because the scan was initiated from deep within the IGZO channel region. As the scan proceeded toward the Al metal contacts, passing through the interface region, the atomic concentrations of In, Ga, and Zn decreased, whereas the Al concentration increased; however, the atomic concentration of oxygen decreased slightly prior to reaching the interface region, as the oxygen atoms had diffused out through the interface. The oxygen concentration increased from the Al$_2$O$_3$ barrier region to the end of the barrier region, then decreased deeper inside the Al metal region. The atomic concentration of the Al metal increased monotonically from just below the interface region to the region deep inside the Al metal layer. IGZO TFTs with a graphene interlayer displayed similar trends for the IGZO constituents (In, Ga, and Zn), although the atomic concentrations of Al and oxygen differed over the transition from the IGZO channel to the Al metal (Figure 4(b)). The oxygen atomic concentration decreased monotonically as the scan proceeded deeper into the Al metal region, whereas the Al concentration increased more sharply

than it was observed in the A-IGZO TFT. The overall Al atomic concentration in the barrier region was much smaller in the IGZO TFTs prepared with a graphene interlayer than in those prepared without this layer. The graphene interlayer apparently prevented the diffusion of oxygen atoms from the IGZO channel into the Al metal contacts, thereby preventing the formation of an Al$_2$O$_3$ barrier region. Figure 4(c) shows a TEM image of the SiO$_2$/IGZO/Al interface regions, indicating the scanning depth from the IGZO channel to the Al metal contact.

In conclusion, stable ohmic behavior at the Al metal contact interface with the IGZO channels was preserved under repeated annealing cycles upon the insertion of a graphene interlayer between the Al metal and the IGZO channel. Graphene was found to provide a perfect barrier for the prevention of oxygen atom diffusion from the IGZO channel into the Al metal contacts, thereby preventing the formation of oxidative layers at the Al/IGZO interface. The present study provides a means for using highly conductive conventional metals to form ohmic contacts with IGZO-based backplane TFTs toward improving the performance of AMOLED displays.

[1] J. H. Seol, I. Jo, A. L. Moore, L. Lindsay, Z. H. Aitken, M. T. Pettes, X. Li, Z. Yao, R. Huang, D. Broido, N. Mingo, R. S. Ruoff, and L. Shi, Science **328**, 213 (2010).
[2] Y. Lee, S. Bae, H. Jang, S. Jang, S. E. Zhu, S. H. Sim, Y. I. Song, B. H. Hong, and J.-H. Ahn, Nano Lett. **10**, 490 (2010).
[3] C. Lee, X. Wei, J. W. Kysar, and J. Hone, Science **321**, 385 (2008).
[4] D. Jiang, V. R. Cooper, and S. Dai, Nano Lett. **9**, 4019 (2009).
[5] J. S. Bunch, S. S. Verbridge, J. S. Alden, A. M. Zande, J. M. Parpia, H. G. Craighead, and P. L. McEuen, Nano Lett. **8**, 2458 (2008).

[6]P. Lange, M. Dorn, N. S. Severin, D. A. Bout, and J. P. Rabe, J. Phys. Chem. C **115**, 23057 (2011).

[7]A. K. Geim and K. S. Novoselov, Nature Mater. **6**, 183 (2007).

[8]O. Leenaerts, B. Partoens, and F. M. Peeters, Appl. Phys. Lett. **93**, 193107 (2008).

[9]S. Chen, L. Brown, M. Levendorf, W. Cail, S.-Y. Ju, J. Edgeworth, X. Li, C. Magnuson, A. Velamakanni, R. Piner, J. Kang, J. Pak, and R. S. Ruoff, ACS Nano **5**, 1321 (2011).

[10]P. Wellenius, A. Suresh, H. Luo, L. M. Lunardi, and J. F. Muth, J. Disp. Technol. **5**, 438 (2009).

[11]S.-H. Park, C.-S. Hwang, M. Ryu, S. Yang, C. Byun, J. Shin, J.-I. Lee, K. Lee, M. S. Oh, and S. Im, Adv. Mater. **21**, 678 (2009).

[12]P. Görrn, M. Sander, J. Meyer, M. Kröger, E. Becker, H.-H. Johannes, W. Kowalsky, and T. Riedl, Adv. Mater. **18**, 738 (2006).

[13]M. Kimura and S. Imai, IEEE Electron Device Lett. **31**, 963 (2010).

[14]T. Hirao, M. Furuta, T. Hiramatsu, T. Matsuda, C. Li, H. Furuta, H. Hokari, M. Yoshida, H. Ishii, and M. Kakegawa, IEEE Trans. Electron Devices **55**, 3136 (2008).

[15]T. Riedl, P. Görrn, and W. Kowalsky, J. Disp. Technol. **5**, 501 (2009).

[16]Y. G. Mo, M. Kim, C. K. Kang, J. H. Jeong, Y. S. Park, C. G. Choi, H. D. Kim, and S. S. Kim, J. Soc. Inf. Disp. **19**, 16 (2011).

[17]H.-W. Zan, W.-W. Tsai, C. H. Chen, and C.-C. Tsai, Adv. Mater. **23**, 4237 (2011).

[18]J. H. Na, M. Kitamura, and Y. Arakawa, Appl. Phys. Lett. **93**, 063501 (2008).

[19]H. Yabuta, M. Sano, K. Abe, T. Aiba, T. Den, H. Kumomi, K. Nomura, T. Kamiya, and H. Hosono, Appl. Phys. Lett. **89**, 112123 (2006).

[20]S. Jeong, Y.-G. Ha, J. Moon, A. Facchetti, and T. J. Marks, Adv. Mater. **22**, 1346 (2010).

[21]C. E. Kim, E. N. Cho, P. Moon, G. H. Kim, D. L. Kim, H. J. Kim, and I. Yun, IEEE Electron Device Lett. **31**, 1131 (2010).

[22]K. Nomura, H. Ohta, A. Takagi, T. Kamiya, H. Hirano, and H. Hosono, Nature **432**, 488 (2004).

[23]S. Yang, J. Y. Bak, S.-M. Yoon, M. K. Ryu, H. Oh, C.-S. Hwang, G. H. Kim, S.-H. K. Park, and J. Jang, IEEE Electron Device Lett. **32**, 1692 (2011).

[24]M. Mativenga, M. H. Choi, and J. W. Choi, IEEE Electron Device Lett. **32**, 170 (2011).

[25]J. Sun, J. Jiang, A. Lu, and Q. Wan, IEEE Trans. Electron Devices **57**, 2258 (2010).

[26]K. H. Cherenack, N. S. Münzenrieder, and G. Tröster, IEEE Electron Device Lett. **31**, 1254 (2010).

[27]J. Liu, D. B. Buchholz, R. P. H. Chang, A. Facchetti, and T. J. Marks, Adv. Mater. **22**, 2333 (2010).

[28]N. Münzenrieder, K. H. Cherenack, and G. Tröster, IEEE Trans. Electron Devices **58**, 2041 (2011).

[29]R. Martins, A. Nathan, R. Barros, L. Pereira, P. Barquinha, N. Correia, R. Costa, A. Ahnood, I. Ferreira, and E. Fortunato, Adv. Mater. **23**, 4491 (2011).

[30]W. Lim, E. A. Douglas, S.-H. Kim, D. P. Norton, S. J. Pearton, and F. Ren, Appl. Phys. Lett. **94**, 072103 (2009).

[31]W. Lim, J. H. Jang, S.-H. Kim, D. P. Norton, V. Craciun, and S. J. Pearton, Appl. Phys. Lett. **93**, 082102 (2008).

[32]H. Kim, J. Y. Moon, Y.-W. Heo, and H. S. Lee, Thin Solid Films **518**, 6348 (2010).

[33]H. Sheng, N. W. Emanetoglu, S. Muthukumar, B. V. Yakshinskiy, S. Feng, and Y. Lu, J. Electron. Mater. **32**, 935 (2003).